

Spatio-temporal correlations can drastically change the response of a MAPK pathway

Koichi Takahashi*

*Advanced Sciences Institute, RIKEN, 1-7-22 Suehirocho, Tsurumi, Yokohama, 230-0045, Japan
The Molecular Sciences Institute, Berkeley, 2168 Shattuck Ave., Berkeley, CA 94704 USA and
Institute for Advanced Biosciences, Keio University, 252-8520 Fujisawa, Japan*

Sorin Tănase-Nicola[†] and Pieter Rein ten Wolde[‡]

*FOM Institute for Atomic and Molecular Physics (AMOLF),
Science park 113, 1098 XG Amsterdam, The Netherlands*

Multisite covalent modification of proteins is omnipresent in eukaryotic cells. A well-known example is the mitogen-activated protein kinase (MAPK) cascade, where in each layer of the cascade a protein is phosphorylated at two sites. It has long been known that the response of a MAPK pathway strongly depends on whether the enzymes that modify the protein act processively or distributively: a distributive mechanism, in which the enzyme molecules have to release the substrate molecules in between the modification of the two sites, can generate an ultrasensitive response and lead to hysteresis and bistability. We study by Green's Function Reaction Dynamics, a stochastic scheme that makes it possible to simulate biochemical networks at the particle level and in time and space, a dual phosphorylation cycle in which the enzymes act according to a distributive mechanism. We find that the response of this network can differ dramatically from that predicted by a mean-field analysis based on the chemical rate equations. In particular, rapid rebindings of the enzyme molecules to the substrate molecules after modification of the first site can markedly speed up the response, and lead to loss of ultrasensitivity and bistability. In essence, rapid enzyme-substrate rebindings can turn a distributive mechanism into a processive mechanism. We argue that slow ADP release by the enzymes can protect the system against these rapid rebindings, thus enabling ultrasensitivity and bistability.

Keywords: MAP kinase — Multisite phosphorylation — Reaction diffusion — Simulation

I. INTRODUCTION

Mitogen-activated-protein kinase (MAPK) cascades are ubiquitous in eukaryotic cells. They are involved in cell differentiation, cell proliferation, and apoptosis [1]. MAPK pathways exhibit very rich dynamics. It has been predicted mathematically and shown experimentally that they can generate an ultrasensitive response [2, 3, 4] and exhibit bistability via positive feedback [5]. It has also been predicted that they can generate oscillations [6, 7, 8], amplify weak but attenuate strong signals [9], and give rise to bistability due to enzyme sequestration [10, 11]. MAPK pathways are indeed important for cell signalling, and for this reason they have been studied extensively, both theoretically [2, 3, 6, 7, 8, 9, 10, 11, 12, 13, 14, 15, 16, 17, 18, 19] and experimentally [2, 4, 5, 7, 16, 20, 21, 22]. However, in most theoretical analyses, the pathway is modelled using chemical rate equations [2, 3, 6, 8, 10, 12, 13, 14, 16]. This is a mean-field description, in which it is assumed that the system is well-stirred and that fluctuations can be neglected. Here, we perform particle-based simulations of one layer of the MAPK cascade using our re-

cently developed Green's Function Reaction Dynamics algorithm [23, 24]. Our simulations reveal that spatio-temporal correlations between the enzyme and substrate molecules, which are ignored in the commonly employed mean-field analyses, can have a dramatic effect on the nature of the response. They can not only speed up the response, but also lead to loss of ultrasensitivity and bistability.

The response time, the sharpness of the input-output relation, and bistability are key functional characteristics of signal transduction pathways. The response time does not only determine how fast a cell can respond to a changing environment, but has also been implicated to underlie many cellular decisions. For example, processes such as cell proliferation and differentiation, selection of T cells, apoptosis, and cell cycle progression are believed to be regulated by the duration of the signal [15, 22, 25, 26, 27, 28, 29]. The sharpness of the input-output relation, or the gain, is a key property of any signal transduction pathway, since it directly affects the signal-to-noise ratio. Bistability can lead to a very sharp, all-or-none response [5], buffer the cell against fluctuations in an input signal, and makes it possible to lock the cell in a given state. Indeed, bistability, or more in general multistability, plays a central role in cell differentiation [30, 31]. It is thus important to understand the mechanisms that underlie bistability, the gain and the response time of MAPK pathways.

A MAPK cascade consists of three layers, where in each layer a kinase activates the kinase of the next layer.

*E-mail: ktakahashi@riken.jp

[†]E-mail: sorin@amolf.nl; Present address: Department of Physics, University of Michigan, Ann Arbor MI 48109-1040

[‡]E-mail: tenwolde@amolf.nl

Importantly, full activation of the kinase requires that it becomes doubly phosphorylated (see Fig. 1). Kinase activation is regulated via a dual phosphorylation cycle, in which the upstream kinase and a phosphatase control the phosphorylation state of the two sites of the kinase in an antagonistic manner. A key question is whether the enzymes that modify the kinase act in a processive or in a distributive manner [2, 3, 4]. In a distributive mechanism, the enzyme has to release the substrate after it has modified the first site, before it can rebind and modify the second site. In contrast, in a processive mechanism, the enzyme remains bound to the substrate in between the modification of the two sites. While a processive mechanism requires only a single enzyme-substrate encounter for the modification of both sites, a distributive mechanism requires at least two enzyme-substrate encounters.

Mean-field analyses based on the chemical rate equations have revealed that whether the enzymes act according to a processive or a distributive mechanism has important functional consequences for the response of a MAPK pathway. A distributive mechanism can generate an ultrasensitive response since the concentration of the fully activated kinase depends quadratically on the upstream kinase concentration [2, 3, 4]. Moreover, if the enzymes are present in limiting amounts, enzyme sequestration can lead to bistable behavior if they act distributively [10]. These mean-field analyses, however, assume that at each instant the molecules are uniformly distributed in space. Here, we show using particle-based simulations that spatio-temporal correlations between the enzyme and the substrate molecules can strongly affect the response of a MAPK pathway.

We perform particle-based simulations of one layer of a MAPK pathway in which the enzymes act according to a distributive mechanism. The simulations reveal that after an enzyme molecule has dissociated from a substrate molecule upon phosphorylation of the first site, it can rebind to the same substrate molecule to modify its second site before another enzyme molecule binds to it. Importantly, the probability per unit amount of time that such a rebinding event occurs does not depend upon the enzyme concentration. As a result, enzyme-substrate rebindings can effectively turn a distributive mechanism into a processive one, even though modification of both sites of a substrate molecule involves at least two collisions with an enzyme molecule. Indeed, a distributive mechanism not only requires a two-collision mechanism, it also requires that the rates at which they occur depend upon the concentration.

These rebindings have important functional consequences. Since rebindings effectively turn a distributive mechanism into a processive one, ultrasensitivity and bistability via enzyme sequestration are lost. Moreover, rebindings strongly reduce the gain of the network. We investigate in depth the scenarios in which rebindings become important. This reveals that the importance of rebindings depends on the concentration and the diffusion constant of the molecules: the lower the concentra-

tion and/or the diffusion constant, the more likely an enzyme molecule rebinds a substrate molecule to modify the second site before another enzyme molecule does. Since enzyme-substrate rebindings are faster than random enzyme-substrate encounters, this observation leads to the counter-intuitive prediction that slower diffusion can lead to a *faster* response. We also find that the impact of rebindings strongly depends on the time it takes to re-activate the enzyme after it has modified the first site. If, for instance, the ADP/ATP exchange on a kinase has to take place after the kinase has dissociated from the substrate upon phosphorylation of the first site, but before it can bind the substrate again to modify the second site, then either slow ADP release or slow ATP supply will make enzyme-substrate rebindings less important. ADP release from protein kinases has been reported to be fairly slow [32], suggesting that slow ADP release might be critical for generating ultrasensitivity and bistability.

The importance of rebindings relies on the interplay between reaction and diffusion at short and long length and time scales. This means that the algorithm should correctly capture the spatio-temporal dynamics of the system at both scales. In this manuscript, we present and apply an enhanced version of our recently developed Green's Function Reaction Dynamics algorithm. This particle-based algorithm is not only even more efficient than the original GFRD scheme, which is already 4 to 5 orders more efficient than brute-force Brownian Dynamics [23], it is also exact.

Biological systems that exhibit macroscopic concentration gradients or spatio-temporal oscillations, which have recently been studied extensively, are typically considered to be reaction-diffusion problems. We believe that our simulations are the first to show that in a biological system that is spatially uniform, spatio-temporal correlations on molecular length scales can drastically change the *macroscopic* behaviour of the system. This underscores the importance of particle-based modelling of biological systems in time and space.

II. MODEL

A. Dual phosphorylation cycle

We consider one layer of the MAPK pathway, consisting of one dual modification cycle, as shown in Fig. 1. Phosphorylation and dephosphorylation proceed via Michaelis-Menten kinetics and according to an ordered, distributive mechanism. Importantly, we assume that the enzymes are inactive after they have released their modified substrate; before they can catalyse the next reaction, they first have to relax back to the active state. The inactive state could reflect that the enzyme is in an inactive conformational state after it has released its product. For the kinase it could also reflect that after it has released its substrate, ADP is bound; only when

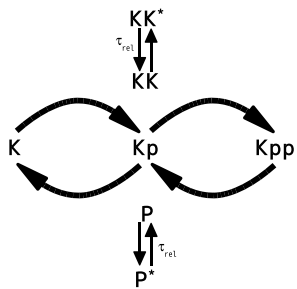
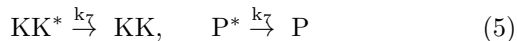
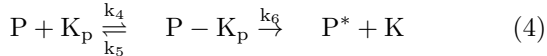
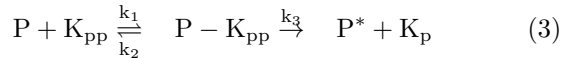
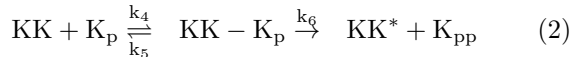
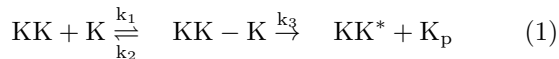


FIG. 1: Dual phosphorylation cycle of one layer of the MAPK cascade. MAPK (K) is activated via double phosphorylation by the kinase MAPKK (KK) of the upstream layer and deactivated via dephosphorylation by a phosphatase (P). It is assumed that the enzymes KK and P act distributively and become inactive (KK* and P*) immediately after the substrate has been modified, relaxing back to the active state with a characteristic time scale τ_{rel} .

ADP has been released and ATP has been bound, does the enzyme become active again. As we will discuss in detail below, the timescale for re-activation, τ_{rel} , plays a key role in the dynamics of the system.

This model is described by the following reactions:



The first two reactions describe the phosphorylation of the kinase of interest, MAPK (K), by the upstream kinase, MAPKK (KK), while Eqs. 3 and 4 describe its dephosphorylation by the phosphatase (P). The inactive state of the enzymes after they have released their product is denoted by the superscript *, and the relaxation towards the active state is described by the last two equations. For simplicity, we assume that re-activation can be described as a simple unimolecular reaction with a time scale $\tau_{\text{rel}} \simeq 1/k_7$. We also assume that the system is symmetric, meaning that the rate constants for the phosphorylation reactions are equal to the corresponding rate constants for the dephosphorylation reactions. We will systematically vary the relaxation time τ_{rel} , and the concentration and the diffusion constant of the particles, D (see below). For the other parameter values, we have taken typical values from the literature (see Methods).

B. Green's Function Reaction Dynamics

We will compare the predictions of a mean-field model based on the chemical rate equations [10] with those of a model in which the particles are explicitly described in time and space. In this particle-based model, it is assumed that the molecules are spherical in shape, have a diameter σ , and move by diffusion with a diffusion constant D . Moreover, two reaction partners can react with each other with an intrinsic rate $k_a = k_1$ or k_4 , respectively, once they are in contact, and two associated species can dissociate with an intrinsic dissociation rate $k_d = k_2$ or k_5 , respectively.

One algorithm to simulate this particle-based model would be Brownian Dynamics. However, since the concentrations are fairly low, much CPU time would be wasted on propagating the reactants towards one another. We therefore employ our recently developed Green's Function Reaction Dynamics algorithm, which uses Green's functions to concatenate the propagation of the particles in space with the chemical reactions between them, allowing for an event-driven algorithm [23, 24] (see Methods).

III. RESULTS

A. Rebindings

To understand the response of the dual phosphorylation cycle, it is critical to consider the distribution of association times for a bimolecular reaction. We consider a simple bimolecular reaction, $A + B \rightleftharpoons C$, where one A molecule can react with one of N B molecules to form a C molecule in a volume V . A model in which it is assumed that the particles are uniformly distributed in space at all times, be it a mean-field continuum or a stochastic discrete model, predicts that this distribution is exponential (see Fig. 2). In contrast, in a spatially-resolved model, the distribution of association times is algebraic on short times and exponential only at later times [33].

The difference between the well-stirred model and the spatially-resolved model is due to rebindings. In a well-stirred model, the propensity that after a dissociation event the A molecule reacts with a B molecule only depends on the total density N/V of B molecules, and not on their positions—in a spatially resolved model this would amount to putting the dissociated B particle to a random position in the cell. Since the total density of B is constant, the association propensity is constant in time, leading to an exponential waiting-time distribution in the well-stirred model. In the spatially resolved model the situation is markedly different. The B molecule that has just dissociated from the A molecule is in close proximity to the A molecule. As a consequence, it can rapidly rebound to the A molecule before it diffuses away from it into the bulk. Such rebindings lead to the algebraic de-

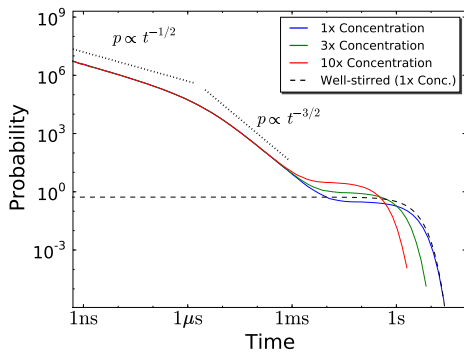


FIG. 2: The distribution of association times for a bimolecular reaction for different concentrations. The system consists of one A molecule that can associate with $N = 10$ B molecules according to the reaction $A + B \xrightleftharpoons[k_d]{k_a} C$. For $t < \tau_{\text{mol}} \approx \sigma^2/D \approx 1\mu\text{s}$ the distribution decays as $t^{-1/2}$, for $\tau_{\text{mol}} < t < \tau_{\text{bulk}} \approx 1\text{s}$ it decays as $t^{-3/2}$, while for $t > \tau_{\text{bulk}}$ the distribution decays exponentially. The algebraic decay is due to rebinding events, in which a dissociated B molecule rebinds the A molecule before diffusing into the bulk; this is unaffected by the concentration of B, [B]. The exponential relaxation is due to B molecules that arrive at A from the bulk, and is a function of [B]. The concentration was controlled by changing the volume from $V = 1, 0.33, \text{ and } 0.1 \mu\text{m}^3$, corresponding to $[B] = N/V = 16, 48, \text{ and } 160 \text{ nM}$, respectively. $k_a = 0.056 \text{ nM}^{-1}\text{s}^{-1}$, $k_d = 1.73 \text{ s}^{-1}$, $D = 1\mu\text{m}^2\text{s}^{-1}$ and $\sigma = 5 \text{ nm}$.

cay of the association-time distribution at short times. For times shorter than the time to travel a molecular diameter, $t < \tau_{\text{mol}} \approx \sigma^2/D$ (see *Supporting Information*), the dissociated B particle essentially experiences a surface of the A particle that is flat, and its rebinding dynamics is given by that of a 1D random walker returning to the origin, leading to the $t^{-1/2}$ decay. At times $\tau_{\text{mol}} < t < \tau_{\text{bulk}}$, the dissociated B particle sees the entire sphere of A, and the probability of a re-encounter event is that of a 3D random walker returning to the origin, decaying as $t^{-3/2}$. At times $t > \tau_{\text{bulk}}$, the dissociated B particle has diffused into the bulk, and it has lost all memory where it came from. The probability that this molecule, or more likely, another B molecule binds the A molecule, now becomes constant in time, leading to an exponential waiting-time distribution at long times [33].

Fig. 2 shows that the association-time distribution depends on the concentration for $t > \tau_{\text{bulk}}$, but not for $t < \tau_{\text{bulk}}$. Indeed, while the encounter rate between two molecules in the bulk depends on their concentration, the rate at which a rebinding event occurs is independent of it. As we will show below, this has major functional consequences for the response of the dual phosphorylation cycle.

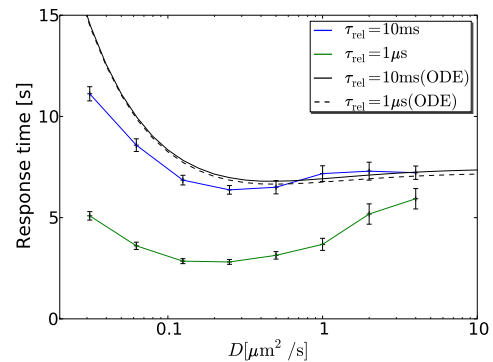


FIG. 3: Average response time as a function of the diffusion constant D for $\tau_{\text{rel}} = 10 \text{ ms}$ (blue line) $\tau_{\text{rel}} = 1 \mu\text{s}$ (green line), as predicted by the particle-based model; for comparison, the predictions of the mean-field model based on the ODE chemical rate equations are also shown (black lines). Initially, only the phosphatases are active; at $t = 0$ the upstream kinases are activated, and plotted is the time it takes on average to reach 50% of the final steady-state level of doubly phosphorylated substrate (Kpp). The optimum in the particle-based model is due to the interplay between phosphorylation of the first site, which slows down with decreasing diffusion constant since enzyme and substrate have to find each other at random, and phosphorylation of the second site, which speeds up with decreasing diffusion constant, because of enzyme-substrate rebindings.

B. Rebindings can speed up the response

Fig. 3 shows the average response time as a function of the diffusion constant, for two different values of the lifetime of the inactive state of the enzymes, τ_{rel} . The figure reveals that both the mean-field (ODE) and the particle-based model predict that there is an optimal diffusion constant that minimizes the response time. However, in the mean-field model the optimum is barely noticeable [47][34]. To a good approximation, the mean-field model predicts that the response time increases with decreasing diffusion constant, because enzyme-substrate association slows down as diffusion becomes slower. In contrast, the particle-based model shows a marked optimum, which is most pronounced when τ_{rel} is short. Clearly, the particle-based simulations predict that slower diffusion can lead to a faster response.

The speed up of the response with slower diffusion is due to the interplay between enzyme-substrate rebindings, and enzyme re-activation. This interplay manifests itself in the distribution of the *second-association time*, defined as the time it takes for a substrate molecule that has just been phosphorylated (Kp) to bind a kinase molecule (KK) for the phosphorylation of the second site (Fig. 4). After a kinase molecule (KK) has phosphorylated the first site of a substrate molecule (K), it will dissociate from it. After dissociation, it is still in close proximity to the substrate molecule, and it will therefore rapidly re-encounter the substrate molecule before

it diffuses away into the bulk. When the lifetime τ_{rel} of the inactive state of the kinase molecule is short compared to the time τ_{mol} it takes for the enzyme and substrate molecule to diffuse away from each other, the probability that upon a re-encounter the enzyme molecule has become active again such that it can actually rebind the substrate molecule, will be large. Hence, when $\tau_{\text{rel}} \leq \tau_{\text{mol}}$, the kinase will often rapidly rebind the substrate molecule, leading to the characteristic algebraic decay of $t^{-3/2}$ for $\tau_{\text{mol}} < t < \tau_{\text{bulk}}$ (Fig. 4A). However, there is also a probability that the enzyme molecule will escape into the bulk before it rebinds the substrate molecule. If this happens, most likely another kinase molecule binds the substrate molecule. This scenario underlies the exponential form of the second-association-time distribution at longer times, with the corner time $\tau_{\text{bulk}} \approx 0.1 - 10$ s. It can now also be understood why the marked peak in the distribution at short times (Fig. 4A) disappears when the enzymes' reactivation time τ_{rel} becomes significantly longer than τ_{mol} (Fig. 4B): after phosphorylation of the first site, the kinase will rapidly re-encounter the substrate molecule many times, but since the enzyme is most probably still inactive, it cannot rebind the substrate molecule, and it will therefore diffuse into the bulk. In the *Supporting Information* we derive analytical expressions for the enzyme-substrate rebinding-time distributions, and elucidate the different scaling regimes that can be observed.

To understand why slower diffusion can lead to a faster response when the lifetime of the enzymes' inactive state is short (Fig. 3), it is instructive to consider how the distribution of second-association times depends on the diffusion constant. Fig. 4A shows that the corner at τ_{bulk} shifts to longer times as the diffusion constant is decreased. This is because the rate at which a kinase molecule from the bulk encounters a given substrate molecule is given by $1/\tau_{\text{bulk}} = k_{\text{D}} = 4\pi\sigma(D_{\text{E}} + D_{\text{S}})[\text{KK}]$, where σ is the sum of the radii of the enzyme and substrate molecules and D_{E} and D_{S} are the diffusion constants of the enzyme and substrate molecules, respectively. Clearly, substrate phosphorylation by kinase molecules that have to find the substrate molecules at random slows down as the molecules move slower. However, the figure also shows that the distribution at the corner time of τ_{bulk} decreases in magnitude while the peak at τ_{mol} increases in magnitude when diffusion becomes slower. This means that as the diffusion constant becomes lower, phosphorylation of the second site is increasingly dominated by enzyme-substrate rebindings rather than by random enzyme-substrate encounters. The probability that the enzyme molecule is still in the vicinity of the substrate molecule after it has relaxed back to the active state, increases as the diffusion constant decreases, making a substrate-rebinding event more likely. This is demonstrated quantitatively in Fig. 4C, which shows the probability that both sites on the substrate are phosphorylated by the same kinase molecule. As expected, this probability not only

increases with decreasing lifetime of the enzymes' inactive state, but also with decreasing diffusion constant. Since enzyme-substrate rebindings are more rapid than random enzyme-substrate encounters, this explains why slower diffusion can lead to a faster response.

While slower diffusion speeds up the modification of the second site by making rapid enzyme-substrate rebindings more likely, it also slows down the modification rate of the first site since that is determined by the rate at which enzyme molecules find the substrate molecules from the bulk. This is the origin of the optimum diffusion constant that minimizes the response time (Fig. 3).

C. Enzyme-substrate rebindings can weaken the sharpness of the response

Fig. 5 shows the effect of enzyme-substrate rebindings on the steady-state input-output relation. It is seen that when the re-activation time of the enzymes is long, $\tau_{\text{rel}} = 10$ ms, the input-output relation is strongly sigmoidal (Fig. 5B). Moreover, it does not depend much on the diffusion constant of the molecules, and it agrees quite well with that predicted by the mean-field model based on the chemical rate equations (Fig. 5B). In contrast, when τ_{rel} is short, *i.e.* $\tau_{\text{rel}} = 1\mu\text{s}$, the input-output relation markedly depends on the diffusion constant (Fig. 5A). For large diffusion constants, the response curve agrees well with that predicted by the mean-field model of a distributive mechanism. But for lower diffusion constants, it increasingly deviates from the mean-field prediction, and it becomes significantly less sigmoidal.

It is commonly believed that multi-site covalent modification can lead to a sigmoidal, cooperative response when the enzymes act distributively, but not when they act processively [2, 35]. While in a distributive scheme modification of n sites of a substrate molecule requires at least n enzyme-substrate binding events, in a processive scheme only one enzyme-substrate binding event is needed. This is often presented as the explanation for why a distributive mechanism enhances the sensitivity of the modification level to changes in enzyme concentration. However, Fig. 5A shows that when the enzymes' re-activation time is short and the species' diffusion constant is low, the input-output relation of a distributive, dual phosphorylation cycle approaches that of a processive, dual phosphorylation cycle. This is due to enzyme-substrate rebindings. Even though during a rebinding trajectory the enzyme molecule is detached from the substrate molecule and two binding events are required for full substrate modification, the rate at which the second site is modified does not depend on the enzyme concentration (Fig. 2). The sharpness of the response increases with the number of required enzyme-substrate binding events, but only when these depend on the enzyme concentration. Enzyme-substrate rebindings effectively turn a distributive mechanism into a processive mechanism.

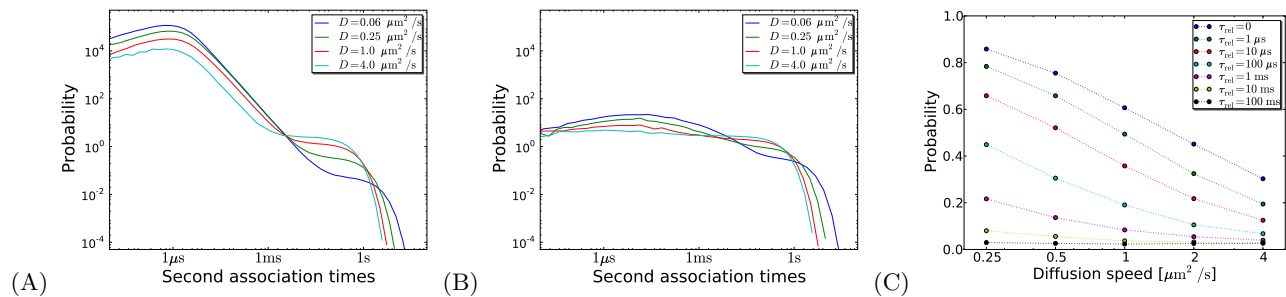


FIG. 4: Distribution of times it takes for a substrate that has just been phosphorylated once (Kp) to bind a kinase molecule (KK), for different diffusion constants. The enzyme reactivation time is (A) $\tau_{\text{rel}} = 1\mu\text{s}$ or (B) $\tau_{\text{rel}} = 10\text{ms}$; in both cases $\tau_{\text{mol}} \approx 1\mu\text{s}$ and $\tau_{\text{bulk}} \approx 0.1 - 10\text{s}$. (C) Probability that the two modification sites of a substrate molecule are phosphorylated by the same kinase molecule as a function of diffusion constant, for different enzyme re-activation times τ_{rel} . It is seen that the probability of an enzyme-substrate rebinding event increases not only with decreasing enzyme reactivation time, but also with decreasing diffusion constant. The latter explains why slower diffusion can lead to a faster response, as seen in Fig. 3.

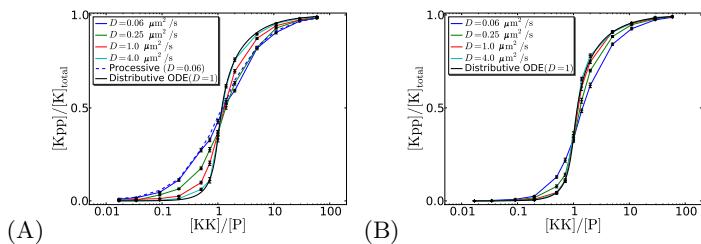


FIG. 5: Steady-state input-output relations for different diffusion constants when (A) $\tau_{\text{rel}} = 1\mu\text{s}$ and (B) $\tau_{\text{rel}} = 10\text{ms}$. For comparison, we also show the predictions of a mean-field (ODE) model of a distributive system with $D = 1\mu\text{m}^2/\text{s}$, and that of a particle-based model of a *processive* system with $D = 0.06\mu\text{m}^2/\text{s}$ (only in panel A). Note that when the reactivation time τ_{rel} is short, the input-output relation of a distributive system approaches that of a processive one as the diffusion constant is lowered (panel A; blue lines).

D. Rebindings can lead to loss of bistability

Markevich *et al.* have shown that bistability can arise in a dual phosphorylation cycle when the enzymes act distributively and are present in limiting concentrations [10]. The idea is that if the substrate molecules are, for example, predominantly unphosphorylated and a substrate molecule is phosphorylated to become singly phosphorylated, it will most likely bind a phosphatase molecule to become unphosphorylated again, instead of a kinase molecule to become fully phosphorylated—when most of the substrate molecules are unphosphorylated, the kinase molecules are mostly sequestered by the unphosphorylated substrate molecules, while the phosphatase molecules are predominantly unbound. However, this is essentially a mean-field argument, which assumes that the substrate and enzyme molecules are randomly distributed in space at all times. Fig. 6 shows that spatio-temporal correlations between the enzyme and substrate molecules can have a dramatic effect on the existence of bistability. When the enzymes' reacti-

vation time τ_{rel} is long, spatio-temporal correlations are not important, and the system indeed exhibits bistability. But when τ_{rel} is short, the probability that a substrate molecule that has just been phosphorylated once will be phosphorylated twice is larger than that it will be dephosphorylated again: the chance that it will rebound the kinase molecule that has just phosphorylated it, will, because of the close proximity of that kinase molecule, be larger than the probability that it will bind a phosphatase molecule, even though in this state there are many more phosphatase than kinase molecules to which the substrate molecule could bind to. These rebindings, or more precisely, spatio-temporal correlations between the enzyme and substrate molecules, are the origin of the loss of bistability when τ_{rel} is short (Fig. 6).

E. The effect of concentration

Figs. 3-6 show that enzyme-substrate rebindings are significant when the concentration of enzyme and substrate is on the order of 100 nM, which is a biologically relevant range [2, 3, 10]. Fig. S4 of the *Supporting Information* shows that when the concentrations of all species are increased by more than a factor 10 from those used in Fig. 5, the system becomes bistable. While the distribution of rebinding times does not depend on the concentration, the competition between phosphatase and kinase molecules in the bulk for binding to the substrate does, in such a way that the system is driven deeper into the bistable regime (see Fig. S5 in *Supporting Information*). Increasing the concentration can thus overcome the effect of enzyme-substrate rebindings.

IV. DISCUSSION

Multi-site phosphorylation is omnipresent in biological systems. Perhaps the best known and arguably the most studied example is the dual phosphorylation cycle of the

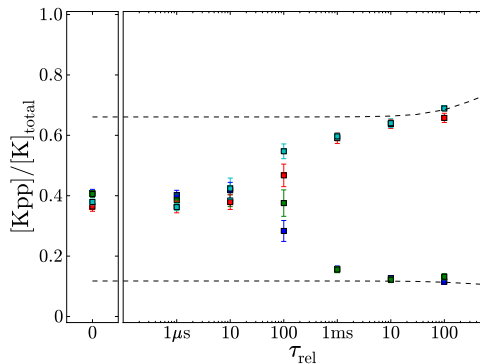


FIG. 6: Relative Kpp concentrations as a function of the lifetime of the inactive state of the enzyme, τ_{rel} . $[K]_{\text{total}} = [Kpp] + [Kp] + [K]$ was increased to 500 nM to bring the system to a regime where the mean-field model based on the chemical rate equations predicts bistability. At each value of τ_{rel} , the particle-based model was simulated until it reaches steady state, starting from four different initial conditions, $[Kpp]/[K]_{\text{total}} = 0$ (blue), 0.3 (green), 0.7 (red), and 1 (cyan). While the mean-field model shows bistability over the whole range of τ_{rel} (black dotted lines), the particle-based model exhibits a bifurcation from mono- to bistability at $t \approx 100 \mu\text{s}$. At this bifurcation point, the system critically slows down, as a result of which it does not even equilibrate after 350 s.

MAPK pathway, studied here, but other well-known examples are the Kai system [36], the CDK inhibitor Sic1 [37], the NFAT system [38], and the CAMKII system [39]. Multi-site phosphorylation can lead to an ultrasensitive response [2, 3], to a threshold response [35], to bistability [10, 39], or synchronise oscillations of phosphorylation levels of individual protein molecules [36], provided the enzymes act via a distributive mechanism. We have studied using a particle-based model a dual phosphorylation cycle in which the enzymes act according to a distributive mechanism. Our results show that rapid enzyme-substrate rebindings can effectively turn a distributive mechanism into a processive mechanism, leading to loss of ultrasensitivity and bistability. Moreover, our results reveal that enzyme-substrate rebindings can significantly speed up the response, with slower diffusion leading to a faster response. While rebindings have been predicted to affect the noise in signal detection [33, 40], our results predict that they can also drastically change the macroscopic behaviour of the system.

Our results reveal that enzyme-substrate rebindings occur on short length and time scales. Rebindings are important up to time scales of about 1 – 10 ms (Fig. 4), corresponding to the time for a protein to diffuse over a few molecular diameters. Beyond those length and time scales the dissociated enzyme and substrate molecules have essentially lost memory where they came from, and they would have to find each other again at random. An important question is whether we should not have taken orientational diffusion into account, precisely because re-

bindings occur at comparable length and time scales. However, the first and second phosphorylation site are often close to each other on the substrate, *e.g.* separated by only a single amino-acid residue [41], suggesting that enzyme-substrate rebindings can indeed occur without significant orientational diffusion. Moreover, our model does not include molecular crowding, and it seems likely that subdiffusion caused by crowding can significantly extend the time scale over which rebindings occur [42].

The importance of enzyme-substrate rebindings depends on the lifetime of the inactive state of the enzymes. For a typical protein diffusion constant of $D = 1-10 \mu\text{m}^2\text{s}^{-1}$ [43, 44, 45], the rebinding probability drops below 10% when the enzyme re-activation time becomes longer than 10 ms (Fig. 4C). Slow enzyme re-activation may thus be critical for generating bistability and ultrasensitivity. To our knowledge, re-activation times of enzymes in MAPK pathways have not been measured yet. The re-activation time of a kinase will depend sensitively on the order in which ADP and modified substrate dissociate from it, and ATP and substrate bind to it. If a kinase can bind its substrate irrespective of the nucleotide binding state, then nucleotide exchange will not be rate limiting. If the ADP is released before the modified substrate, but ATP binding is required for binding of the next substrate, then ATP binding might be the rate-limiting step; with mM ATP concentrations, this is however expected to yield fast re-activation times, of order microseconds. If the modified substrate must dissociate before ADP can dissociate and ADP must dissociate before the kinase can bind substrate again, then the rate of ADP release may become rate limiting. A recent study on a protein kinase provides support for the latter scenario, with an ADP release rate that is on the order of 100ms [32]. This suggests that slow ADP release may allow for ultrasensitivity and bistability, although more work is needed to explore these mechanisms in depth. Concerning bistability, it is possible that bistability requires the phosphatase to act distributively [10]. Bistability could thus be lost if the mechanism by which the phosphatase acts changes from a distributive to a processive mechanism due to rebindings. To our knowledge, it is unknown what the minimum time is to re-activate a phosphatase. It is conceivable that this time is very short. Rapid re-activation of the phosphatase could thus lead to loss of bistability.

Our results show that experiments to determine whether an enzyme acts distributively or processively should be interpreted with care. These experiments are often performed by investigating the time courses of the concentrations of the intermediate and final products [4]. If the amount of intermediate products exceeds that of the enzyme, then the mechanism must be distributive. However, our results reveal that the converse does not necessarily imply that the mechanism is processive, as commonly assumed: enzyme-substrate rebindings can turn a distributive mechanism into a processive one, with the concentration of the intermediate product remain-

ing below that of the enzyme. We stress that the question whether an enzyme acts processively because of rebindings or because it remains physically attached to the substrate is biologically relevant, because the importance of enzyme-substrate rebindings strongly depends on the conditions. It depends on the diffusion constants of the components, the lifetime of the inactive state of the enzyme, and on the concentrations of the components. All these factors may vary from one place in the cell to another and will vary from one cell to the next. In fact, an enzyme that operates according to a distributive mechanism in the test-tube may act processively in the crowded environment of the cell.

Finally, how could our predictions be tested experimentally? If the enzyme of interest is a kinase, then one experiment would be to change the lifetime of the inactive state by varying the ATP concentration or by making mutations that change the ADP release rate. Another proposal would be to study the enzyme kinetics as a function of the concentration of a crowding agent, such as PEG [32]. Crowding will slow down diffusion, and will, because of subdiffusion [42], increase the time that an enzyme and a substrate molecule that are in close proximity, stay together. Both effects will make enzyme-substrate rebindings more likely. Studying the input-output relation and the time course of the intermediate and final products [4, 32] for different levels of macromolecular crowding will shed light on the importance of spatio-temporal correlations for the macroscopic behavior of biological systems employing multi-site modifications.

V. METHODS

A. Green's Function Reaction Dynamics

A reaction-diffusion system is a many-body problem that can not be solved analytically. The key idea of GFRD is to decompose the many-body problem into single and two-body problems, which can be solved analytically using Green's functions [23, 24]. These Green's functions are then used to set up an event-driven algorithm, which makes it possible to make large jumps in time and space when the particles are far apart from each other. In the original version of the algorithm, the many-body problem was solved by determining at each iteration of the simulation a maximum time step such that each particle could interact with at most one other particle during that time step [23, 24]. In the enhanced version of the algorithm presented here, called eGFRD, spherical protective domains are put around single and

pairs of particles [46]. This allows for an exact, asynchronous event-driven algorithm (see *Supporting Information*).

B. MAPK model

The model of the distributive, MAP kinase dual phosphorylation cycle is sketched in Fig. 1 and described by Eqs. 1-5. The rate constants are $k_1 = 0.027 \text{ nM}^{-1} \cdot \text{s}^{-1}$, $k_2 = 1.35 \text{ s}^{-1}$, $k_3 = 1.5 \text{ s}^{-1}$, $k_4 = 0.056 \text{ nM}^{-1} \cdot \text{s}^{-1}$, $k_5 = 1.73 \text{ s}^{-1}$, $k_6 = 15.0 \text{ s}^{-1}$, $k_7 = \ln 2 / \tau_{\text{rel}}$. The protein diameter $\sigma = 5 \text{ nm}$. k_1 and k_4 are the intrinsic association rates, which are the association rates for two species in contact; k_2 and k_5 are the intrinsic dissociation rates [33]. While in the particle-based model the diffusion of the particles is simulated explicitly, in the mean-field model based on the ODE chemical rate equations, diffusion is described implicitly by renormalizing the association and dissociation rates [33]: $1/k_{\text{on}} = 1/k_a + 1/k_D$ and $1/k_{\text{off}} = 1/k_d + K_{\text{eq}}/k_D$, where k_{on} and k_{off} are the renormalized association and dissociation rates, respectively, $k_a = k_1, k_4$ and $k_d = k_2, k_5$ are the respective intrinsic association and dissociation rates, $k_D = 4\pi\sigma D$ is the diffusion-limited association rate, and $K_{\text{eq}} = k_a/k_d = k_{\text{on}}/k_{\text{off}}$ is the equilibrium constant. The particles were put in a cubic volume of $1 \mu\text{m}^3$ with periodic boundary conditions. The total enzyme concentration $[\text{KK}] + [\text{P}]$ is 100 nM corresponding to 60 copies of molecules in the volume, and the total substrate concentration $[\text{K}] + [\text{Kp}] + [\text{Kpp}]$ is 200 nM or 120 copies of molecules in Figs 3, 4 and 5, and 500 nM or 300 copies of molecules in Fig 6. The processive model consists of the following six reactions, sharing the same rate constants as the distributive model: $\text{KK} + \text{K} \xrightleftharpoons[k_2]{k_1, k_2} \text{KK} - \text{K} \xrightleftharpoons[k_5]{k_3} \text{KK} - \text{K}_p \xrightleftharpoons[k_6]{k_4} \text{KK} + \text{K}_{pp}$, $\text{P} + \text{K}_{pp} \xrightleftharpoons[k_7]{k_1, k_2} \text{P} - \text{K}_{pp} \xrightleftharpoons[k_6]{k_3} \text{P} - \text{K}_p \xrightleftharpoons[k_6]{k_6} \text{P} + \text{K}$.

Acknowledgments

KT conducted part of the research as a Human Frontier Science Program Cross-Disciplinary Fellow at the Molecular Sciences Institute. We thank Marco Morelli, Jeroen van Zon, Boris Kholodenko, Tom Shimizu, Frank Bruggeman and Steven Andrews for useful discussions, Moriyoshi Koizumi for help in implementation, and Institute for Advanced Biosciences of Keio University for computing facility. The work is part of the research program of the "Stichting voor Fundamenteel Onderzoek der Materie (FOM)", which is financially supported by the "Nederlandse organisatie voor Wetenschappelijk Onderzoek (NWO)".

[1] Chang, L, Karin, M (2001) Mammalian map kinase signalling cascades. *Nature* 410:37–40.

[2] Huang, CYF, Ferrell, JE, Jr. (1996) Ultrasensitivity in the mitogen-activated protein kinase cascade. *Proc Natl*

Acad Sci USA 93:10078 – 10083.

- [3] Ferrell, JE, Jr. (1996) Tripping the switch fantastic: how a protein kinase cascade can convert graded inputs into switch-like outputs. *Trends Biochem Sci* 21:460–466.
- [4] Ferrell, JE, Jr., Bhatt, RR (1997) Mechanistic studies of the dual phosphorylation of mitogen-activated protein kinase. *J Biol Chem* 272:19008–19016.
- [5] Ferrell, JE, Jr., Machleder, EM (1998) The biochemical basis of an all-or-none cell fate switch in xenopus oocytes. *Science* 280:895–898.
- [6] Kholodenko, BN (2000) Negative feedback and ultrasensitivity can bring about oscillations in the mitogen-activated protein kinase cascades. *Eur J Biochem* 267:1583–1588.
- [7] Wang, X, Hao, N, Dohlman, HG, Elston, TC (2006) Bistability, stochasticity, and oscillations in the mitogen-activated protein kinase cascade. *Biophys J* 90:1961–1978.
- [8] Chickarmane, V, Kholodenko, BN, Sauro, HM (2007) Oscillatory dynamics arising from competitive inhibition and multisite phosphorylation. *J Theor Biol* 244:68–76.
- [9] Locasale, JW, Shaw, AS, Chakraborty, AK (2007) Scaffold proteins confer diverse regulatory properties to protein kinase cascades. *Proc Natl Acad Sci U S A* 104:13307–13312.
- [10] Markevich, NI, Hoek, JB, Kholodenko, BN (2004) Signaling switches and bistability arising from multisite phosphorylation in protein kinase cascades. *J Cell Biol* 164:353–359.
- [11] Elf, J, Ehrenberg, M (2004) Spontaneous separation of bi-stable biochemical systems into spatial domains of opposite phases. *Syst Biol (Stevenage)* 1:230–236.
- [12] Levchenko, A, Bruck, J, Sternberg, PW (2000) Scaffold proteins may biphasically affect the levels of mitogen-activated protein kinase signaling and reduce its threshold properties. *Proc Natl Acad Sci U S A* 97:5818–5823.
- [13] Heinrich, R, Neel, BG, Rapoport, TA (2002) Mathematical models of protein kinase signal transduction. *Mol Cell* 9:957–970.
- [14] Angeli, D, Ferrell, JE, Jr, Sontag, ED (2004) Detection of multistability, bifurcations, and hysteresis in a large class of biological positive-feedback systems. *Proc Natl Acad Sci U S A* 101:1822–1827.
- [15] Locasale, JW, Chakraborty, AK (2008) Regulation of signal duration and the statistical dynamics of kinase activation by scaffold proteins. *PLoS Comput Biol* 4:e1000099.
- [16] Hornberg, JJ et al. (2005) Principles behind the multifarious control of signal transduction. erk phosphorylation and kinase/phosphatase control. *FEBS J* 272:244–258.
- [17] Qiao, L, Nachbar, RB, Kevrekidis, IG, Shvartsman, SY (2007) Bistability and oscillations in the huang-ferrell model of mapk signaling. *PLoS Comput Biol* 3:1819–1826.
- [18] Tănase-Nicola, S, Warren, PB, ten Wolde, PR (2006) Signal detection, modularity, and the correlation between extrinsic and intrinsic noise in biochemical networks. *Phys Rev Lett* 97:068102–1–4.
- [19] Berezhkovskii, AM, Coppey, M, Shvartsman, SY (2009) Signaling gradients in cascades of two-state reaction-diffusion systems. *Proc Natl Acad Sci U S A* 106:1087–1092.
- [20] Burack, WR, Sturgill, TW (1997) The activating dual phosphorylation of mapk by mek is nonprocessive. *Biochemistry* 36:5929–5933.
- [21] Zhao, Y, Zhang, ZY (2001) The mechanism of dephosphorylation of extracellular signal-regulated kinase 2 by mitogen-activated protein kinase phosphatase 3. *J Biol Chem* 276:32382–32391.
- [22] Santos, SDM, Verveer, PJ, Bastiaens, PIH (2007) Growth factor-induced mapk network topology shapes erk response determining pc-12 cell fate. *Nat Cell Biol* 9:324–330.
- [23] van Zon, JS, ten Wolde, PR (2005) Simulating biochemical networks at the particle level and in time and space: Green’s function reaction dynamics. *Phys Rev Lett* 94:128103.
- [24] van Zon, JS, ten Wolde, PR (2005) Green’s-function reaction dynamics: A particle-based approach for simulating biochemical networks in time and space. *J Chem Phys* 123:234910.
- [25] Marshall, CJ (1995) Specificity of receptor tyrosine kinase signaling: transient versus sustained extracellular signal-regulated kinase activation. *Cell* 80:179–185.
- [26] Chen, YR, Wang, X, Templeton, D, Davis, RJ, Tan, TH (1996) The role of c-jun n-terminal kinase (jnk) in apoptosis induced by ultraviolet c and gamma radiation. duration of jnk activation may determine cell death and proliferation. *J Biol Chem* 271:31929–31936.
- [27] Fischle, W, Verdine, E, Greene, WC (2001) Duration of nuclear nf-kappaB action regulated by reversible acetylation. *Science* 293:1653–1657.
- [28] Murphy, LO, Smith, S, Chen, RH, Fingar, DC, Blenis, J (2002) Molecular interpretation of erk signal duration by immediate early gene products. *Nat Cell Biol* 4:556–564.
- [29] Murphy, LO, Blenis, J (2006) Mapk signal specificity: the right place at the right time. *Trends Biochem Sci* 31:268–275.
- [30] Gilbert, SF (2003) *Developmental Biology* (Sinauer Associates, Inc.).
- [31] Manu, Surkova, S et al. (2009) Canalization of gene expression and domain shifts in the drosophila blastoderm by dynamical attractors. *PLoS Comput Biol* 5:e1000303.
- [32] Keshwani, MM, Harris, TK (2008) Kinetic mechanism of fully activated s6k1 protein kinase. *J Biol Chem* 283:11972–11980.
- [33] van Zon, JS, Morelli, M, Tănase-Nicola, S, ten Wolde, PR (2006) Diffusion of transcription factors can drastically enhance the noise in gene expression. *Biophys J* 91:4350–4367.
- [34] Agmon, N and Szabo, A (1990) Theory of reversible diffusion-influenced reactions. *J Chem.Phys* 92:5270 – 5284.
- [35] Gunawardena, J (2005) Multisite protein phosphorylation makes a good threshold but can be a poor switch. *Proc Natl Acad Sci U S A* 102:14617–14622.
- [36] van Zon, JS, Lubensky, DK, Altena, PRH, ten Wolde, PR (2007) An allosteric model of circadian kaic phosphorylation. *Proc Natl Acad Sci U S A* 104:7420–7425.
- [37] Nash, P et al. (2001) Multisite phosphorylation of a cdk inhibitor sets a threshold for the onset of dna replication. *Nature* 414:514–521.
- [38] Crabtree, GR, Olson, EN (2002) Nfat signaling: choreographing the social lives of cells. *Cell* 109 Suppl:S67–79.
- [39] Miller, P, Zhabotinsky, AM, Lisman, JE, Wang, XJ (2005) The stability of a stochastic camkii switch: dependence on the number of enzyme molecules and protein turnover. *PLoS Biol* 3:e107.
- [40] Andrews, SS (2005) Serial rebinding of ligands to clus-

- tered receptors as exemplified by bacterial chemotaxis. *Physical Biology* 2:111–122.
- [41] Payne, DM et al. (1991) Identification of the regulatory phosphorylation sites in pp42/mitogen-activated protein kinase (map kinase). *EMBO J* 10:885–892.
- [42] Lomholt, MA, Zaid, IM, Metzler, R (2007) Subdiffusion and weak ergodicity breaking in the presence of a reactive boundary. *Phys Rev Lett* 98:200603.
- [43] Elowitz, MB, Surette, MG, Wolf, PE, Stock, JB, Leibler, S (1999) Protein mobility in the cytoplasm of *Escherichia coli*. *J Bacteriol* 181:197–203.
- [44] Meacci, G et al. (2006) Mobility of min-proteins in *Escherichia coli* measured by fluorescence correlation spectroscopy. *Phys Biol* 3:255–263.
- [45] Elf, J, Li, GW, Xie, XS (2007) Probing transcription factor dynamics at the single-molecule level in a living cell. *Science* 316:1191–1194.
- [46] Opplestrup, T, Bulatov, VV, Gilmer, GH, Kalos, MH, Sadigh, B (2006) First-passage monte carlo algorithm: diffusion without all the hops. *Phys Rev Lett* 97:230602.
- [47] The optimum is due to the fact that when a substrate molecule is bound to an enzyme molecule, the probability $k_3/(k_2+k_3)$ that it is modified by the enzyme molecule instead of dissociating from it, slightly increases with decreasing diffusion constant (the dissociation rate k_2 decreases with decreasing D).

Supporting Information

Spatio-temporal correlations can drastically change the response of the MAPK pathway

K. Takahashi, S. Tănase-Nicola and P. R. ten Wolde

November 10, 2021

Contents

1	Enhanced Green's Function Reaction Dynamics	2
1.1	Overview	2
1.2	Single particle events	2
1.3	Particle pair events	4
1.4	Algorithm outline	6
2	Rebinding-time distribution	8
3	The effect of concentration	12

arXiv:0907.0514v1 [q-bio.MN] 3 Jul 2009

1 Enhanced Green's Function Reaction Dynamics

1.1 Overview

We present the enhanced Green's Function Reaction Dynamics (eGFRD) simulation algorithm. We provide the concepts required to understand the outline of the algorithm, but details on the algorithm, such as the actual mathematical expression for the employed Green's functions, other numerical procedures, and performance analyses, will be given in a forthcoming publication [1].

We solve the many-body reaction-diffusion problem by decomposing it into a set of many one body (single) and two body (pair) problems, for which analytical solutions (Green's functions) exist. In the original version of the GFRD algorithm, the many-body problem was solved by determining at each step of the simulation a maximum time step Δt such that each particle could interact with at most one other particle during that time step. In practice, the maximum time step Δt was determined as follows: 1) an interaction sphere of radius $H\sqrt{6D_i\Delta t}$ is drawn around each particle, where D_i is the diffusion constant of the i -th particle, and H is a user-set error control parameter (usually 3 or 4); 2) the maximum time step Δt is then set by the requirement that each interaction sphere overlaps at most with one other interaction sphere. Subsequently, for each single particle and pair of particles a tentative reaction time is drawn, after which all particles are propagated simultaneously up to the smallest tentative reaction time, or to the maximum time step if that is smaller than the smallest tentative reaction time [2, 3]. Although already up to five orders more efficient than conventional reaction Brownian Dynamics [4] and also very accurate by its own right, the original GFRD algorithm has three major drawbacks; 1) due to the synchronous nature, the decomposition into one and two-body problems has to happen at every simulation step; 2) all components in the system are propagated according to the smallest tentative reaction time, making the performance sub-optimum; 3) the decomposition into single particles and pairs of particles involves cut-off distances, which makes the algorithm inexact. The systematic error is controlled by the H parameter, which determines the probability that during a time step Δt a particle travels a distance further than the maximum distance set by the requirement that each particle can interact with at most one other particle. This means that there is a trade-off between performance and error.

In the current work, we overcome the drawbacks of the original GFRD scheme by putting protective domains around single particles and pairs of particles [5]. In this scheme, the next event of a domain can either be a reaction, or one particle leaving the domain. The tentative exit time for the latter event is computed by imposing an absorbing boundary condition on the surface of the protective domain. This makes the algorithm exact, and allows for an asynchronous event-driven algorithm.

In the following sections, we explain how the reaction-diffusion problem in a spherical protective domain is solved for the one-body (Single problem) and two-body case (Pair problem), and then describe how the simulations of the different domains are integrated.

1.2 Single particle events

We consider a single particle of diameter d surrounded by a spherical protective shell of radius a (Fig. S1(A)). Motion of a freely diffusing spherical particle is described by the Einstein diffusion equation,

$$\partial_t p_1(\mathbf{r}, t | \mathbf{r}_0, t_0) = D \nabla^2 p_1(\mathbf{r}, t | \mathbf{r}_0, t_0), \quad (1)$$

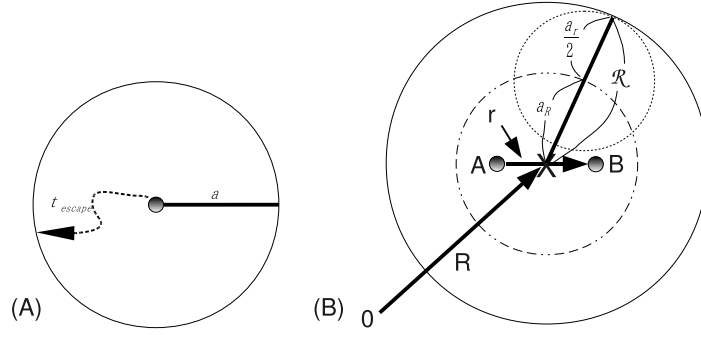


Figure S1: Single and Pair objects. To solve the many-body problem exactly, protective domains are put around single particles (A) and pairs of particles (B). (A) The radius of the protective domain of a single particle is denoted by a . (B) To solve the reaction-diffusion problem of two particles that can react with each other and diffuse within a protective domain with radius \mathcal{R} , we construct two protective domains: one for the center-of-mass \mathbf{R} , with radius a_R , and one for the inter-particle vector \mathbf{r} , with radius a_r . The radii a_R and a_r can be freely chosen, provided that when \mathbf{R} and \mathbf{r} would reach their maximum lengths, i.e. when $|\mathbf{R}| = a_R$ and $|\mathbf{r}| = a_r$, the particles A and B would remain within the protective domain. The latter means that a_R and a_r should satisfy the following two constraints: 1) $a_R + a_r D_A / (D_A + D_B) < \mathcal{R} - \sigma_A / 2$, which reflects that particle A should remain with the protective domain with radius \mathcal{R} ; 2) $a_R + a_r D_B / (D_A + D_B) < \mathcal{R} - \sigma_B / 2$, reflecting that B should remain with the protective domain with radius \mathcal{R} . Although a_R and a_r can be freely chosen provided that these constraints are met, an efficient choice is given by $a_R^2 / D_R^2 = (a_r - \mathbf{r}_0)^2 / D_r^2$, meaning that the average time for \mathbf{R} to reach the boundary of its domain by free diffusion, equals that of \mathbf{r} . To illustrate the constraints, panel B shows a scenario where \mathbf{R} and \mathbf{r} reach their maximum lengths; here, $D_A = D_B$.

where the Green's function $p_1(\mathbf{r}, t | \mathbf{r}_0, t_0)$ denotes the probability that the particle is at position \mathbf{r} at time t given that it was at \mathbf{r}_0 at time t_0 . We obtain the Green's function $p_1(\mathbf{r}, t | \mathbf{r}_0, t_0)$ by solving the diffusion equation, Eq. 1, with the following initial and boundary conditions

$$p_1(\mathbf{r}, t_0 | \mathbf{r}_0, t_0) = \delta(\mathbf{r} - \mathbf{r}_0), \quad (2)$$

$$p_1(|\mathbf{r} - \mathbf{r}_0| = a, t | \mathbf{r}_0, t_0) = 0, \quad (3)$$

where δ denotes the Dirac delta function.

From the Green's function one can obtain the survival probability

$$S_1(t | \mathbf{r}_0, t_0) = \int_{|\mathbf{r} - \mathbf{r}_0| < a} d\mathbf{r} p_1(\mathbf{r}, t | \mathbf{r}_0, t_0), \quad (4)$$

which is the probability at time t that the particle remains within the protective sphere of radius a . This is related to the probability per unit time that the particle escapes the domain for the first time,

$$q_1^{\text{escape}}(t | \mathbf{r}_0, t_0) = -\partial S(t | \mathbf{r}_0, t_0) / \partial t. \quad (5)$$

Sampling from this escape-propensity function yields a tentative escape time t_{escape} .

It is also possible that the particle undergoes a unimolecular reaction. The probability that the next reaction happens in an infinitesimal time interval t and $t + dt$ is [6]

$$q_1^{\text{reaction}}(t | t_0) dt = k \exp(-k(t - t_0)) dt, \quad (6)$$

where k is the first-order reaction rate. This distribution can be used to obtain the next tentative reaction time t_{reaction} .

The next event time of a *Single* is given by the smallest of the two tentative event times, namely,

$$t_{\text{single}} = \min(t_{\text{escape}}, t_{\text{reaction}}). \quad (7)$$

1.3 Particle pair events

To describe the diffusion and the reaction of a pair of particles, we use the distribution function $p_2(\mathbf{r}_A, \mathbf{r}_B, t | \mathbf{r}_{A0}, \mathbf{r}_{B0}, t_0)$, which gives the probability that the particles A and B are at positions \mathbf{r}_A and \mathbf{r}_B at time t , given that they were at \mathbf{r}_{A0} and \mathbf{r}_{B0} at time t_0 . This distribution function satisfies for $|\mathbf{r}| \geq \sigma$, where $\sigma = (d_A + d_B)/2$ is the cross-section with d_A and d_B the diameters of particles A and B , respectively, the following diffusion equation:

$$\partial_t p_2(\mathbf{r}_A, \mathbf{r}_B, t | \mathbf{r}_{A0}, \mathbf{r}_{B0}, t_0) = [D_A \nabla_A^2 + D_B \nabla_B^2] p_2(\mathbf{r}_A, \mathbf{r}_B, t | \mathbf{r}_{A0}, \mathbf{r}_{B0}, t_0). \quad (8)$$

We aim to solve this equation for two particles that can react with each other and diffuse within a protective domain. To our knowledge, it is impossible to solve this equation and obtain the Green's function directly. We therefore apply the following tricks.

First, we make a coordinate transformation

$$\mathbf{R} \equiv \frac{D_B \mathbf{r}_A + D_A \mathbf{r}_B}{D_A + D_B}, \quad (9)$$

$$\mathbf{r} \equiv \mathbf{r}_B - \mathbf{r}_A, \quad (10)$$

and define the operators

$$\nabla_{\mathbf{R}} \equiv \partial / \partial \mathbf{R}, \quad (11)$$

$$\nabla_{\mathbf{r}} \equiv \partial / \partial \mathbf{r}. \quad (12)$$

Eq. 8 can then be rewritten as:

$$\partial_t p_2(\mathbf{R}, \mathbf{r}, t | \mathbf{R}_0, \mathbf{r}_0, t_0) = [D_R \nabla_{\mathbf{R}}^2 + D_r \nabla_{\mathbf{r}}^2] p_2(\mathbf{R}, \mathbf{r}, t | \mathbf{R}_0, \mathbf{r}_0, t_0), \quad (13)$$

where $D_R \equiv D_A D_B / (D_A + D_B)$ and $D_r \equiv D_A + D_B$. This equation describes two independent random processes, one for the inter-particle vector \mathbf{r} and another for the center-of-mass vector \mathbf{R} . This means that the distribution function $p_2(\mathbf{r}_A, \mathbf{r}_B, t | \mathbf{r}_{A0}, \mathbf{r}_{B0}, t_0)$ can be factorized as $p_2^{\mathbf{R}}(\mathbf{R}, t | \mathbf{R}_0, t_0) p_2^{\mathbf{r}}(\mathbf{r}, t | \mathbf{r}_0, t_0)$ and that the above equation can be reduced to one diffusion equation for the coordinate \mathbf{R} and another for the coordinate \mathbf{r} :

$$\partial_t p_2^{\mathbf{R}}(\mathbf{R}, t | \mathbf{R}_0, t_0) = D_R \nabla_{\mathbf{R}}^2 p_2^{\mathbf{R}}(\mathbf{R}, t | \mathbf{R}_0, t_0), \quad (14)$$

$$\partial_t p_2^{\mathbf{r}}(\mathbf{r}, t | \mathbf{r}_0, t_0) = D_r \nabla_{\mathbf{r}}^2 p_2^{\mathbf{r}}(\mathbf{r}, t | \mathbf{r}_0, t_0). \quad (15)$$

The crux is now to define one protective domain for the interparticle vector \mathbf{r} , with radius a_r , and another for the center-of-mass vector \mathbf{R} , with radius a_R (see Fig. S1(B)). These domains have to be chosen such that when the inter-particle vector \mathbf{r} and the center-of-mass vector \mathbf{R} would reach their maximum lengths, given by $|\mathbf{r}| = a_r$ and $|\mathbf{R}| = a_R$, respectively, the particles A and B would still be within the protective domain for the two particles.

The diffusion equation for the center-of-mass vector now has to be solved with the boundary conditions

$$p_2^{\mathbf{R}}(\mathbf{R}, t_0 | \mathbf{R}_0, t_0) = \delta(\mathbf{R} - \mathbf{R}_0), \quad (16)$$

$$p_2^{\mathbf{R}}(|\mathbf{R} - \mathbf{R}_0| = a_R, t | \mathbf{R}_0, t_0) = 0. \quad (17)$$

This problem, of the center-of-mass diffusing in its protective domain, is similar to that of the single particle diffusing in a protective domain as discussed in the previous section. From the corresponding propensity function $q_2^{\mathbf{R}}(t | \mathbf{r}_0)$ we can draw a tentative time t_R at which the center-of-mass leaves its protective domain.

The solution for the diffusion equation for the inter-particle vector is less trivial, since it should take into account not only that the inter-particle vector can leave its protective domain, but also that the two particles can react with each other. This reaction is included as an extra boundary condition, yielding the following boundary conditions for the inter-particle vector \mathbf{r} :

$$p_2^{\mathbf{r}}(\mathbf{r}, t_0 | \mathbf{r}_0, t_0) = \delta(\mathbf{r} - \mathbf{r}_0), \quad (18)$$

$$p_2^{\mathbf{r}}(|\mathbf{r}| = a_r, t | \mathbf{r}_0, t_0) = 0, \quad (19)$$

$$-j(\sigma, t | \mathbf{r}_0, t_0) \equiv 4\pi\sigma^2 D_r \frac{\partial}{\partial r} p_2^{\mathbf{r}}(\mathbf{r}, t | \mathbf{r}_0, t_0) |_{|\mathbf{r}|=\sigma} = k_a p_2^{\mathbf{r}}(|\mathbf{r}| = \sigma, t | \mathbf{r}_0, t_0), \quad (20)$$

where $\partial/\partial r$ denotes a derivative with respect to the inter-particle separation r . Eq. 20 is the boundary condition that describes the possibility that A and B can react with a rate k_a once they are in contact. Here, $j(\sigma, t | \mathbf{r}_0, t_0)$ is the radial flux of probability $p_2^{\mathbf{r}}(\mathbf{r}, t | \mathbf{r}_0, t_0)$ through the “contact” surface of area $4\pi\sigma^2$. This boundary condition, also known as a *radiation* boundary condition [7], states that this radial flux of probability equals the intrinsic rate constant k_a times the probability that the particles A and B are in contact. In the limit $k_a \rightarrow \infty$, the radiation boundary condition reduces to an *absorbing* boundary condition $p_2^{\mathbf{r}}(|\mathbf{r}| = \sigma, t | \mathbf{r}_0, t_0) = 0$, while in the limit $k_a \rightarrow 0$ the radiation boundary condition reduces to a *reflecting* boundary condition.

From the Green’s function for the inter-particle vector \mathbf{r} , $p_2^{\mathbf{r}}(\mathbf{r}, t | \mathbf{r}_0, t_0)$, we can obtain two important quantities. The first is the time t_{bimo} at which the inter-particle vector crosses the reaction surface given by $|\mathbf{r}| = \sigma$ —meaning that the particles A and B react with each other—and the other is the time t_r at which it “escapes” through the boundary of the protective domain given by $|\mathbf{r}| = a_r$. The time at which the next event happens, be it a reaction or an escape, can be obtained through the survival probability, which is given by

$$S_2^{\mathbf{r}}(t | \mathbf{r}_0, t_0) = \int_{\sigma \leq |\mathbf{r}| < a_r} d\mathbf{r} p_2^{\mathbf{r}}(\mathbf{r}, t | \mathbf{r}_0, t_0). \quad (21)$$

The propensity function $q_2^{\mathbf{r}}(t | \mathbf{r}_0, t_0)$, which is the probability that the next event happens between time t and $t + dt$, is related to the survival probability by

$$q_2^{\mathbf{r}}(t | \mathbf{r}_0, t_0) \equiv -\frac{\partial S_2^{\mathbf{r}}(t | \mathbf{r}_0, t_0)}{\partial t}. \quad (22)$$

To know which of the two event types, reaction or escape, happens at time t , we split this quantity into two components,

$$q_2^{\mathbf{r}}(t | \mathbf{r}_0, t_0) = q_2^{\sigma}(t | \mathbf{r}_0, t_0) + q_2^{a_r}(t | \mathbf{r}_0, t_0) \quad (23)$$

$$= \int_{|\mathbf{r}|=\sigma} dS D_r \frac{\partial}{\partial r} p_2^{\mathbf{r}}(\mathbf{r}, t | \mathbf{r}_0, t_0) - \int_{|\mathbf{r}|=a_r} dS D_r \frac{\partial}{\partial r} p_2^{\mathbf{r}}(\mathbf{r}, t | \mathbf{r}_0, t_0), \quad (24)$$

where in the first term dS denotes an integral over the reaction surface at $|\mathbf{r}| = \sigma$, and in the second term an integral over the boundary of the protective domain $|\mathbf{r}| = a_r$. The reaction rate $q_2^\sigma(t|\mathbf{r}_0, t_0)$ is the probability that the *next* reaction for a pair of particles, initially separated by \mathbf{r}_0 , occurs at time t , while the escape rate $q_2^{a_r}(t|\mathbf{r}_0, t_0)$ yields the probability that the inter-particle distance reaches a_r and escapes from the protective domain for the first time at time t . We can draw the tentative time t for the next event, be it an escape or a reaction event, from Eq. 22, and then determine which of the two takes place from the ratio of $q_2^\sigma(t|\mathbf{r}_0, t_0)$ and $q_2^{a_r}(t|\mathbf{r}_0, t_0)$ at time t . Alternatively, we can draw a tentative time for a bimolecular reaction, t_{bimo} , from $q_2^\sigma(t|\mathbf{r}_0, t_0)$ and a tentative time for an escape event, t_r , from $q_2^{a_r}(t|\mathbf{r}_0, t_0)$; which of the two events can occur is then the one with the smallest tentative time (see below). The function $\frac{\partial}{\partial \mathbf{r}} p_2^{\mathbf{r}}(\mathbf{r}, t|\mathbf{r}_0, t_0)$ can be used to sample the exit points on the relevant surfaces.

It is possible that the particles A and B do not only react with each other, but also can undergo a unimolecular reaction of the type $X \rightarrow \dots$. In the same way as in the *Single* problem (Eq. 6), we can also draw the times $t_{\text{mono},A}$ and $t_{\text{mono},B}$ at which the particles A and B undergo a first-order reaction, respectively.

The next event of a pair of particles in a protective domain is thus one of the following events: 1) the center-of-mass leaving its domain; 2) the inter-particle event leaving its domain; 3) a bimolecular reaction; 4) unimolecular reaction of molecule A; 5) a unimolecular reaction of molecule B. The event that actually takes place is the one with the smallest tentative time. The next event time for a protective domain with two particles is thus given by

$$t_{\text{pair}} = \min(t_R, t_r, t_{\text{bimo}}, t_{\text{mono},A}, t_{\text{mono},B}). \quad (25)$$

1.4 Algorithm outline

The outline of the eGFRD algorithm is given by:

1. *Initialize*: Reset the simulator time ($t_{\text{sim}} \leftarrow 0$). For each particle in the system, draw a spherical protective domain of appropriate size. When two particles are very close, create a *Pair* between them. Otherwise, create a *Single* object for each of the particles. Then, for each of the *Single* and the *Pair* objects, draw the next event type and the next event time according to the formulations in the previous sections, and chronologically order the events in the scheduler.
2. *Step*: Pick the next event with the smallest scheduled time t from the scheduler. Update the simulator time $t_{\text{sim}} \leftarrow t$.
 - *Single event*
 - If the event is a *Single escape* event, then (1) propagate the particle to a randomly determined exit point on the surface of the protective domain; (2) check if there are protective domains that are close to the new position of the particle; (3) if there are, burst the neighboring domains, and propagate the particles in the burst domains to a new position, and check if the current *Single* particle can form a *Pair* with one of the neighboring particles; (4) if a *Pair* is formed, discard the current *Single*, determine the new *Pair* event time (Eq. 25), and schedule the new *Pair* event on the scheduler; (5) for each of the particles contained in the stepping *Single* or the burst domains that are not used in formation of the *Pair*, draw a new domain and schedule a *Single* event on the scheduler.

- If the event type is *Single reaction*, (1) propagate the particle to a point \mathbf{r} within the protective domain according to the *Single* Green’s function $p_1(\mathbf{r}, t_{\text{sim}} | \mathbf{r}_{\text{last}}, t_{\text{last}})$, where t_{last} is the time the *Single* was created or the last time it stepped, and \mathbf{r}_{last} is the position of the particle at t_{last} ; (2) execute the reaction by replacing the particle with one or more of the product particles placed next to each other; (3) for each of the newly created particles, draw a new protective domain and schedule a *Single event* on the scheduler.
- *Pair event*
 - If the event type is *Pair reaction*, meaning that the two particles in the domain react, (1) draw the new \mathbf{R} from $p_2^{\mathbf{R}}(\mathbf{R}, t_{\text{sim}} | \mathbf{R}_{\text{last}}, t_{\text{last}})$, where \mathbf{R}_{last} is the position of \mathbf{R} at t_{last} , which is the time at which the *Pair* was formed; (2) remove particles A and B of the *Pair* from the simulator; (3) place the product particle(s) at the new position \mathbf{R} ; (4) draw protective domain(s) around the new particle(s), and schedule *Single* event(s) on the scheduler.
 - If the event type was *r escape*, meaning that the inter-article vector \mathbf{r} leaves its protective domain, (1) sample the new \mathbf{R} position as above; (2) sample the \mathbf{r} exit point from $\frac{\partial}{\partial \mathbf{r}} p_2^{\mathbf{r}}$; (3) determine the new positions of A and B, \mathbf{r}_A and \mathbf{r}_B , by putting the \mathbf{R} as calculated in (1), and the exit point \mathbf{r} on the surface of the inter-particle protective domain as calculated in (2), into Eqs 9 and 10; (4) delete the *Pair*; (5) create a *Single* domain and schedule a new *Single* event on the scheduler for both A and B.
 - If the event type is *R escape*, meaning that the center-of-mass leaves its domain, (1) sample the new inter-particle vector \mathbf{r} with $p_2^{\mathbf{r}}(\mathbf{r}, t_{\text{sim}} | \mathbf{r}_{\text{last}}, t_{\text{last}})$, where \mathbf{r}_{last} is the inter-particle vector at the time t_{last} it was last updated; (2) sample the \mathbf{R} exit point from $\frac{\partial}{\partial \mathbf{r}} p_2^{\mathbf{R}}$; (3) displace the particles A and B to the new positions; (4) delete the *Pair*; (5) create two *Singles* and schedule them on the scheduler.
 - If the event type was *single reaction*, (1) burst the pair domain and update the positions of the particles A and B by sampling $p_2^{\mathbf{R}}(\mathbf{R}, t_{\text{sim}} | \mathbf{R}_{\text{last}}, t_{\text{last}})$ and $p_2^{\mathbf{r}}(\mathbf{r}, t_{\text{sim}} | \mathbf{r}_{\text{last}}, t_{\text{last}})$; (2) execute the reaction of the reacting particle according to the same procedures as used in the *Single* event; (3) create a new *Single* domain for the other (non-reacting) particle and schedule it on the scheduler.

3. Go to 2.

It can happen that more than two particles come very close to each other, making it difficult to draw protective domains of sufficient size around each of the particles[5]; this could bring the simulations to a standstill. To preempt this scenario, the algorithm puts one protective domain around the “squeezed” particles to form a third type of object called *Multi*. The particles in this domain are propagated according to Brownian dynamics[4] until the particles recover from the squeezed condition. Since it is guaranteed that Brownian dynamics converges to the correct solution when a sufficiently small step size is used[4], this squeezing recovery procedure does not affect the overall accuracy of the simulation.

The actual forms of the single and pair Green’s functions, efficient numerical evaluation methods for the Green’s functions, more details on the algorithm including the recovery procedure from squeezing, and handling of surfaces will be described in a forthcoming publication [1].

2 Rebinding-time distribution

In this section we present scaling relations for the rebinding-time distributions of two particles that can diffuse and react with each other in a large compartment. These results give a mathematical interpretation of the non-monotonic form of the enzyme-substrate rebinding-time distributions, shown in Fig. 4 (panels A and B) of the main text.

The problem is reduced to solving the reaction-diffusion equation for a random walker that can diffuse in a domain internally bounded by a sphere of radius σ , and to which it can bind with an intrinsic rate k_a once it is in contact with the sphere. This represents the evolution of the inter-particle vector \mathbf{r} describing the distance between a substrate molecule and the enzyme molecule that has just modified it.

The rebinding probability can be obtained from the Green's function $p_2(\mathbf{r}, t | \mathbf{r}_0, t_0)$. The probability that a particle that starts at the origin given by $|\mathbf{r}| = \sigma$ returns to the origin at a later time t , is given by

$$p_2(\sigma, t | \sigma, 0) = \frac{\sigma - e^{Dt/\sigma^2(1+h\sigma)^2} \sqrt{\pi Dt} (1+h\sigma) \operatorname{erfc}\left((1+h\sigma)\sqrt{\frac{Dt}{\sigma^2}}\right)}{4\pi\sigma^3\sqrt{\pi Dt}}, \quad (26)$$

where erfc is the complementary error function. If we assume that the enzyme becomes active immediately after enzyme-substrate dissociation, then, according to Eq. 20, the rebinding-time probability distribution can be expressed as

$$p_{\text{reb}}^0(t) = k_a p_2(\sigma, t | \sigma, 0). \quad (27)$$

This rebinding-time distribution has a number of properties. Firstly, the total probability that there is a rebinding is smaller than one:

$$\int_0^\infty dt p_{\text{reb}}(t) = \frac{1}{1 + \frac{4\pi D\sigma}{k_a}} < 1. \quad (28)$$

Secondly, upon a variable change $t = \tau \frac{\sigma^2}{D(1+k_a/(4\pi D\sigma))^2}$, the rebinding probability distribution can be rescaled as

$$p_{\text{reb}}(\tau) = \frac{1}{1 + \frac{4\pi D\sigma}{k_a}} f(\tau), \quad f(\tau) = \left[\frac{1}{\sqrt{\pi\tau}} - e^\tau \operatorname{erfc}(\sqrt{\tau}) \right]. \quad (29)$$

The function $f(\tau)$ has the shape of two power laws $f(\tau) \simeq \frac{1}{\sqrt{\tau}}$ for $\tau \ll 1$ and $f(\tau) \simeq \frac{1}{\tau\sqrt{\tau}}$ for $\tau \gg 1$, in accordance with the results presented in Figure 2 of the main text. In fact, we can estimate the time for the inflection point to be $\tau_{\text{mol}} = \frac{\sigma^2}{D(1+k_a/(4\pi D\sigma))^2}$. Here, τ_{mol} represents the time after which most of the rebindings correspond to particles that start at contact, but wander away from the reaction sphere before they return to and rebind the reaction sphere. We stress that these trajectories are *rebinding* trajectories: we thus exclude trajectories where particles diffuse in the bulk and come back in a memory-less fashion (see also below). The $t^{-1/2}$ scaling for $t < \tau_{\text{mol}}$ can be understood by noticing that on this time scale particles stay close to the surface of the reaction sphere; indeed, on this time scale the particles essentially see a flat reaction surface, meaning that the return-time distribution is that of a 1D random walker as described in the main text. The $t^{-3/2}$ scaling for $t > \tau_{\text{mol}}$ can be understood by observing that on this time scale the particles have diffused away from the surface of the sphere; the particles now see the entire sphere, which means that the rebinding-time distribution is that of a 3D random walker returning to the origin. Interestingly, τ_{mol} depends on k_a . When k_a is increased, the probability that a particle binds

the target upon contact increases. Hence, the probability that after a time t the particle is still performing a 1D random walk close to the surface, decreases as k_a increases—the particle has either reacted with the surface, or escaped from the surface, thus performing a 3D random walk.

So far we have assumed that upon dissociation, the enzyme and substrate can rebind as soon as they are in contact again. If, however, they can only rebind after the enzyme has become active again, then the rebinding-time distribution is given by

$$p_{\text{reb}}(t) = \int_0^t dt' \int_{\sigma}^{\infty} 4\pi r^2 dr p_2^*(r, t' | \sigma, 0) k_a p_{\text{act}}(t') p_2(\sigma, t - t' | r, 0), \quad (30)$$

where

$$p_{\text{act}}(t) = k_{\text{act}} e^{-k_{\text{act}} t} \quad (31)$$

is the enzyme reactivation distribution with $k_{\text{act}} \equiv 1/\tau_{\text{rel}}$, and $p_2^*(r, t | r_0, 0)$ is the solution of the Smoluchowski equation with a reflecting boundary condition—this reflects the idea that when the enzyme has not become active yet, the substrate cannot bind it.

While we do not know an analytical expression for the rebinding-time distribution of Eq. 30, we can derive a lower bound $p_{\text{reb}}^{\text{min}}(t)$ and an upper bound $p_{\text{reb}}^{\text{max}}(t)$ for it, such that $p_{\text{reb}}^{\text{min}}(t) \leq p_{\text{reb}}(t) \leq p_{\text{reb}}^{\text{max}}(t)$. The upper bound $p_{\text{reb}}^{\text{max}}(t)$ is based on the inequality

$$p_2(\sigma, t - t' | r, 0) \leq p_2(\sigma, t - t' | \sigma, 0), \quad (32)$$

with equality for $r = \sigma$. This inequality expresses the fact that the probability that the particles are in contact at a later time t decreases with the initial distance. This yields the upper bound

$$p_{\text{reb}}^{\text{max}}(t) = \int_0^t dt' k_a p_{\text{act}}(t') p_2(\sigma, t - t' | \sigma, 0). \quad (33)$$

Using the solution for $p_2(\sigma, t - t' | \sigma, 0)$ as described in 29 one can show that for small t the bound increases with t as \sqrt{t} , while for large t it decreases with t as $\frac{1}{t\sqrt{t}}$. The upper bound $p_{\text{reb}}^{\text{max}}(t)$ thus has a non-monotonic behavior, going to zero at both zero and infinity. The position of the maximum depends on the two time scales $\tau_{\text{rel}} = 1/k_{\text{act}}$ and τ_{mol} and is located in the interval $[\text{MIN}(\tau_{\text{mol}}, \tau_{\text{rel}}), \text{MAX}(\tau_{\text{mol}}, \tau_{\text{rel}})]$.

The lower bound $p_{\text{reb}}^{\text{min}}(t)$ is based on the inequality $p_2(r, t | \sigma, 0) \leq p_2^*(r, t | \sigma, 0)$. This reflects the idea that with a radiation boundary condition, the particle can react with the reactive sphere (and thus leak out of the system), while with a reflecting boundary condition it cannot. This yields the following expression for the lower bound

$$p_{\text{reb}}^{\text{min}}(t) = \int_0^t dt' k_a p_{\text{act}}(t') p_2(\sigma, t | \sigma, 0), \quad (34)$$

$$= (1 - e^{-k_{\text{act}} t}) k_a p_2(\sigma, t | \sigma, 0), \quad (35)$$

$$= s_{\text{act}}(t) p_{\text{reb}}^0(t), \quad (36)$$

where $s_{\text{act}}(t)$ is the probability that the enzyme is active after time t and $p_{\text{reb}}^0(t)$ is the enzyme-substrate rebinding-time distribution assuming that the enzyme is active at all times. This lower bound has a number of interesting scaling regimes, depending on the relative values of τ_{rel} and τ_{mol} . They can be understood intuitively by making the following observations: as discussed above, for $t < \tau_{\text{mol}}$, $p_{\text{reb}}^0(t) \sim t^{-1/2}$, while for $t > \tau_{\text{mol}}$, $p_{\text{reb}}^0(t) \sim t^{-3/2}$; moreover, for $t \ll \tau_{\text{rel}}$, $s_{\text{act}}(t) \sim t$, while for $t \gg \tau_{\text{rel}}$, $s_{\text{act}}(t) \rightarrow 1$. Hence, for $t < \text{MIN}(\tau_{\text{mol}}, \tau_{\text{rel}})$, $p_{\text{reb}}^{\text{min}}(t) \sim t^{-1/2} \times t \sim t^{+1/2}$, while for $t > \text{MAX}(\tau_{\text{mol}}, \tau_{\text{rel}})$, $p_{\text{reb}}^{\text{min}}(t) \sim t^{-3/2}$. Moreover, when $\tau_{\text{rel}} < \tau_{\text{mol}}$, $p_{\text{reb}}^{\text{min}}(t) \sim t^{-1/2}$ for $\tau_{\text{rel}} < t < \tau_{\text{mol}}$,

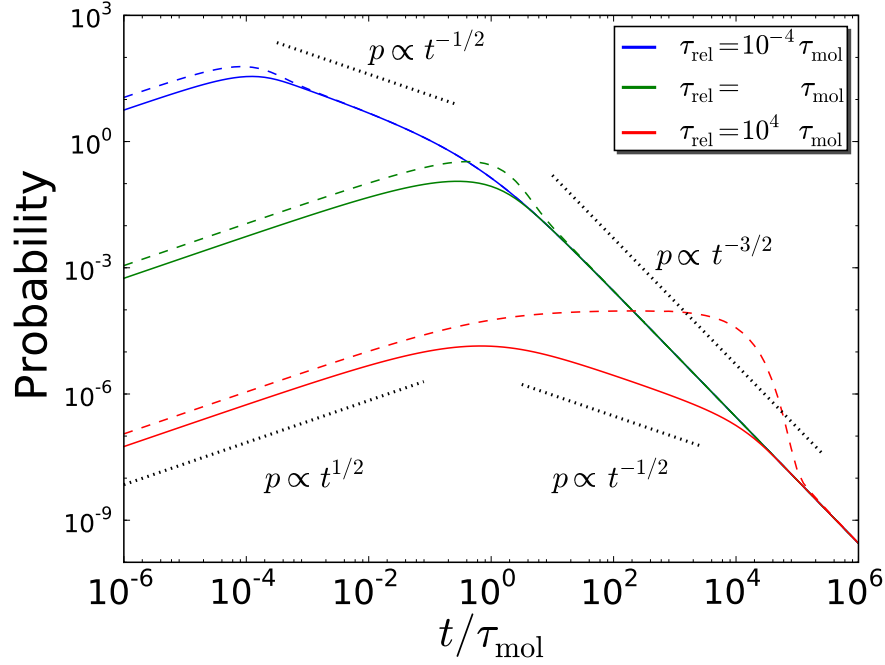


Figure S2: The upper bound Eq. 33 (dashed lines) and lower bound Eq. 36 (solid lines) of the rebinding-time distribution, given by Eq. 30, for three different scenarios: 1) $\tau_{\text{rel}} \ll \tau_{\text{mol}}$ (blue lines); $\tau_{\text{rel}} \approx \tau_{\text{mol}}$ (green lines); $\tau_{\text{rel}} \gg \tau_{\text{mol}}$ (red lines). It is seen that both bounds converge when $t > \tau_{\text{rel}}$. It is also seen that the difference between the bounds is rather small when $t < \tau_{\text{mol}}$. The difference between the upper and lower bounds arises for $\tau_{\text{mol}} < t < \tau_{\text{rel}}$, when $\tau_{\text{rel}} \gg \tau_{\text{mol}}$ (red lines). This is because in this case the reactive sphere (*i.e.*, enzyme) is mostly still inactive, and the (substrate) particle thus tends to diffuse away from it. This phenomenon is captured by the lower bound, but not by the upper bound. For a comparison with the simulation results, see Fig. S3.

because $s_{\text{act}} \rightarrow 1$ and $p_{\text{reb}}^0(t) \sim t^{-1/2}$. And in the scenario that $\tau_{\text{mol}} < \tau_{\text{rel}}$, $p_{\text{reb}}^{\text{min}}(t) \sim t^{-1/2}$ for $\tau_{\text{mol}} < t < \tau_{\text{rel}}$, because $s_{\text{act}} \sim t$ and $p_{\text{reb}}^0(t) \sim t^{-3/2}$.

Fig. S2 shows the predictions of the upper bound Eq. 33 and lower bound Eq. 36 for the rebinding-time distribution given by Eq. 30, for three different scenarios: 1) $\tau_{\text{rel}} \ll \tau_{\text{mol}}$ (blue line); 2) $\tau_{\text{rel}} \approx \tau_{\text{mol}}$ (green line); 3) $\tau_{\text{rel}} > \tau_{\text{mol}}$ (red line). It is seen that in all 3 scenarios the upper and lower bound for $p_{\text{reb}}(t)$ converge for $t > \tau_{\text{rel}}$. Indeed, in this regime, where the enzyme is active, $p_{\text{reb}}(t)$ scales as $t^{-3/2}$. It is also observed that when $\tau_{\text{rel}} \leq \tau_{\text{mol}}$ (blue and green lines), the difference between the upper and lower bound for $p_{\text{reb}}(t)$ is very small, even when $t < \tau_{\text{rel}}$. This implies that both bounds are good approximations for $p_{\text{reb}}(t)$; we can thus conclude that, to a good approximation, $p_{\text{reb}}(t)$ scales as $t^{1/2}$ for $t < \text{MIN}(t_{\text{rel}}, \tau_{\text{mol}})$ and $t^{-1/2}$ for $\tau_{\text{rel}} < t < \tau_{\text{mol}}$ when $\tau_{\text{rel}} < \tau_{\text{mol}}$. The difference between the bounds arises when $\tau_{\text{rel}} > \tau_{\text{mol}}$ (red line); in this scenario, the bounds differ in the regime $\tau_{\text{mol}} < t < \tau_{\text{rel}}$. The question arises which bound is closer to the actual rebinding-time distribution, $p_{\text{reb}}(t)$. To this end, we compare our analytical results with the simulation data, shown in Fig. S3.

In Fig. S3 we show the simulation results of Fig.4 of the main text. When $t \geq \tau_{\text{bulk}}$ the rebinding-time distribution is exponential. This is due to particles that come from the bulk, and bind the reactive sphere in a memory-less fashion. This regime is not described by the analysis

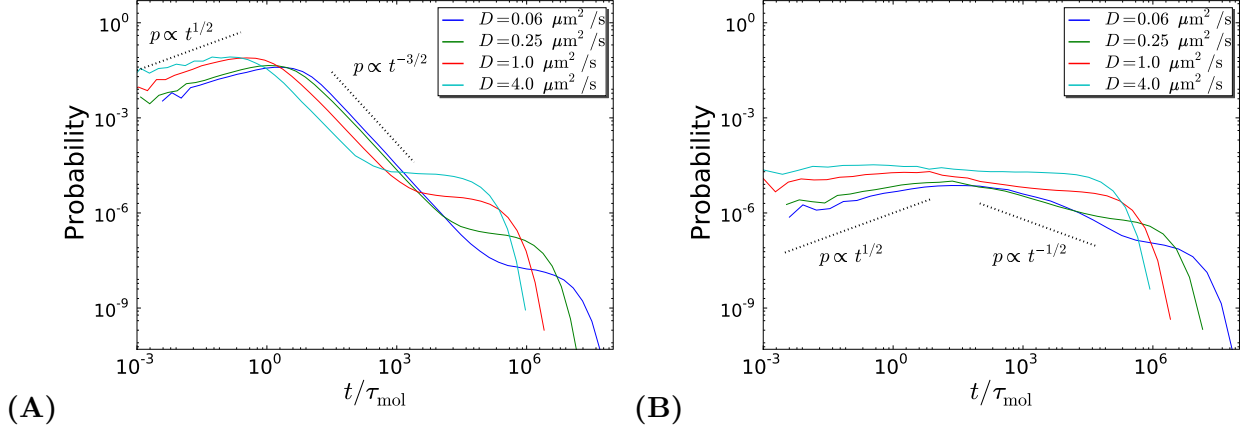


Figure S3: The enzyme-substrate association-time distribution of Fig. 4 of the main text, together with the scaling regimes as predicted by the analysis of the upper and lower bounds for the rebinding-time distribution (see Fig. S2); in panel A $\tau_{\text{rel}} \approx \tau_{\text{mol}}$, while in panel B $\tau_{\text{rel}} \gg \tau_{\text{mol}}$. For $t > \tau_{\text{bulk}}$, the association-time distribution is exponential, because on this time scale the particles meet each other at random in the bulk. As predicted by the analysis of the upper and lower bounds for the rebinding-time distribution (see Fig. S2), the enzyme-substrate association-time distribution scales as $t^{1/2}$ for $t < \text{MIN}(\tau_{\text{mol}}, \tau_{\text{rel}})$, and as $t^{-3/2}$ for $\text{MAX}(\tau_{\text{mol}}, \tau_{\text{rel}}) < t < \tau_{\text{bulk}}$; while the $t^{1/2}$ scaling is seen in both panels, the $t^{-3/2}$ is only seen in panel A, because in panel B τ_{bulk} approaches τ_{rel} . Panel B shows that the lower bound Eq. 36 correctly predicts the $t^{-1/2}$ scaling for $\tau_{\text{mol}} < t < \tau_{\text{rel}}$, when $\tau_{\text{rel}} \gg \tau_{\text{mol}}$.

discussed above, which is performed for the geometry of an infinite, spherical domain internally bounded by a reactive sphere. For this geometry, in three dimensions, there is a probability that the particle escapes to infinity without returning to and reacting with the reactive sphere. In a bounded domain, when a particle escapes from the vicinity of the reactive sphere into the bulk, it will return to the reactive sphere on a time scale τ_{bulk} . Therefore, the rebinding-time distributions for the infinite domain analyzed above and the finite domain of the simulations, are the same, but only up to τ_{bulk} . This also means that to observe the different power-law scaling behaviours, $\tau_{\text{bulk}} \gg \text{MAX}(\tau_{\text{rel}}, \tau_{\text{mol}})$.

In panel A of Fig. S3, $\tau_{\text{rel}} \approx \tau_{\text{mol}}$, while in panel B $\tau_{\text{rel}} \gg \tau_{\text{mol}}$. In both scenarios $p_{\text{reb}}(t) \sim (t)^{1/2}$ when $t < \text{MIN}(\tau_{\text{rel}}, \tau_{\text{mol}})$, in accordance with the analysis of the upper and lower bounds of $p_{\text{reb}}(t)$ presented above. Both panels also show that when $\text{MAX}(\tau_{\text{mol}}, \tau_{\text{rel}}) < t < \tau_{\text{bulk}}$, $p_{\text{reb}}(t) \sim t^{-3/2}$. An interesting regime is $\tau_{\text{mol}} < t < \tau_{\text{rel}}$ in the case that $\tau_{\text{rel}} > \tau_{\text{mol}}$ (panel B). It is seen that the simulation results suggest that $p_{\text{reb}}(t) \sim t^{-1/2}$ in this regime. This is predicted by the lower bound for $p_{\text{reb}}(t)$, Eq. 36, but not by the upper bound, Eq. 33 (see Fig. S2). This can be understood by noting that in this regime, $\tau_{\text{mol}} < t < \tau_{\text{rel}}$, the enzyme is mostly still inactive and the particle can thus diffuse away from the reactive sphere; while the lower bound of Eq. 36 captures this effect, the upper bound of Eq. 33 does not, since it is based on the inequality $p_2(\sigma, t-t'|r, 0) \leq p_2(\sigma, t-t'|\sigma, 0)$.

3 The effect of concentration

Fig. S4 shows the input-output relation as a function of concentration. Here, the concentrations of all components are increased by the same factor from the base-line values used in Fig.5A of the main text. It is seen that both the particle-based model and the mean-field model predict that an increase in concentration induces bistability, although the concentration at which the bifurcation occurs is higher in the particle-based model.

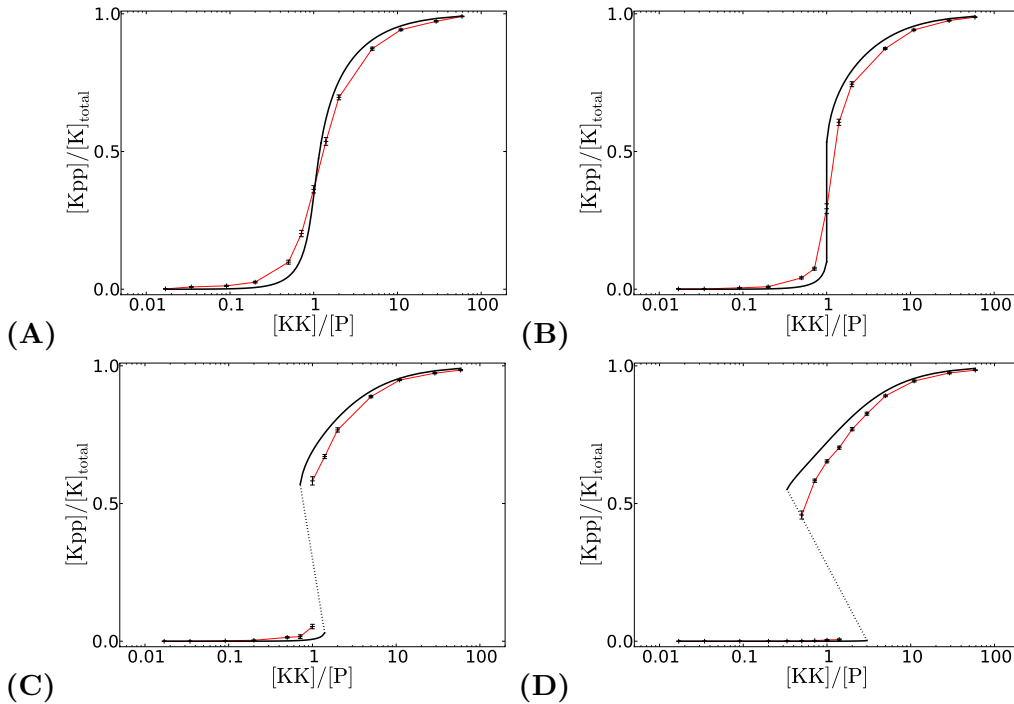


Figure S4: Steady-state input-output relations for different concentrations. The concentrations of all components are increased by the same factor. (A) Baseline parameter values; the concentrations equal those corresponding to Fig. 5(A) in the main text: $[K]_{\text{total}} = 200\text{nM}$, $[KK] + [P] = 100\text{nM}$. (B) 3x concentration ($[K]_{\text{total}} = 600\text{nM}$, $[KK] + [P] = 300\text{nM}$), (C) 10x concentration ($[K]_{\text{total}} = 2\mu\text{M}$, $[KK] + [P] = 1\mu\text{M}$), (D) 100x concentration ($[K]_{\text{total}} = 20\mu\text{M}$, $[KK] + [P] = 10\mu\text{M}$).

Fig. S5 elucidates the origin of why an increase in concentration can induce bistability, both in the mean-field model and the particle-based model. Bistability arises when a substrate molecule that has been phosphorylated once, is more likely to be dephosphorylated again than to become fully phosphorylated (similarly, the probability that after a fully phosphorylated molecule has been dephosphorylated once becomes fully phosphorylated again, should be higher than that it becomes fully dephosphorylated). We therefore plot in Fig. S5 the probability that a substrate that has just been phosphorylated once, either binds the same kinase molecule as the one that just phosphorylated it (this is most likely due to a rebinding event), another kinase molecule (from the bulk), or a phosphatase molecule (from the bulk); the system is in a state where most substrate molecules are unphosphorylated. It is seen that the fraction of rebindings is fairly constant. This can be understood as follows: 1) the probability that a molecule returns to the origin before it loses memory where it came from is independent of the concentration (see Fig.2 of the main text)—only the memory-less returns from the bulk depend on concentration; 2) when a rebinding event happens, it happens very fast: as Fig. 2 of the main text shows, rebindings are dominated

by events that occur on time scales of $t < 1$ ms. These time scales are so short, that the probability that an enzyme molecule from the bulk interferes with a rebinding event, is negligible, even up to concentrations of 100-1000 times the baseline value, i.e. $10 - 100 \mu\text{M}$; only above that concentration can molecules from the bulk effectively compete with those undergoing a rebinding trajectory, and will the probability that a dissociated molecule rebinds drop significantly. Up to a concentration of $10 - 100 \mu\text{M}$, there is thus an essentially constant probability, independent of the concentration, that both sites of a substrate molecule are modified by the same enzyme molecule. Now bistability can arise when the antagonistic enzyme in the bulk wins the competition from the agonistic enzyme undergoing the rebinding event and the other agonistic enzymes in the bulk. Fig. S5 shows that when the concentration is increased, the competition between the kinase (the agonist) in the bulk and the phosphatase (antagonist) in the bulk changes in favor of the phosphatase. This is because the system is in a state where the substrate molecules are mostly unphosphorylated, and in this state the kinase molecules become increasingly sequestered by the unphosphorylated substrate molecules as the concentration is increased. This increases the probability that a molecule that has just been phosphorylated once, will bind a phosphatase (antagonist), which will drive it back towards the unphosphorylated state. Increasing the overall concentration thus changes the competition between the kinases and the phosphatases in the bulk in such a way that the driving force towards a state in which the substrate molecules are either fully unphosphorylated or fully phosphorylated, increases. In essence, increasing the concentration drives the system deeper into the bistable regime. This makes it possible to overcome the effect of rebindings, which tends to drive the system out of the bistable regime, as shown in Fig. 6 of the main text.

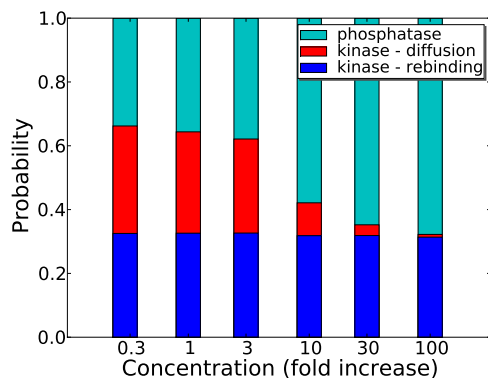


Figure S5: The probability that a substrate molecule that has been phosphorylated once, will bind the same kinase molecule (blue), another kinase molecule (red) or a phosphatase molecule (green), for difference concentrations; the baseline values correspond to Fig.5A of the main text and Fig. S4. It is seen that the fraction of events where the substrate molecule binds the same kinase molecule again is fairly constant, while the fraction of events in which the substrate molecule binds another kinase molecule strongly drops in favor of those in which the substrate molecule binds a phosphatase molecule, when the concentration is increased by a factor 10 from the baseline value—as shown in Fig. S4, the system now becomes bistable.

References

- [1] Takahashi, K, Tănase-Nicola, S, ten Wolde, PR (2009) in preparation.

- [2] van Zon, JS, ten Wolde, PR (2005) Simulating biochemical networks at the particle level and in time and space: Green's function reaction dynamics. *Phys Rev Lett* 94:128103.
- [3] van Zon, JS, ten Wolde, PR (2005) Green's-function reaction dynamics: A particle-based approach for simulating biochemical networks in time and space. *J Chem Phys* 123:234910.
- [4] Morelli, MJ, Tănase-Nicola, S, Allen, RJ, ten Wolde, PR (2008) Reaction coordinates for the flipping of genetic switches. *Biophys J* 94:3413 – 3423.
- [5] Opplestrup, T, Bulatov, VV, Gilmer, GH, Kalos, MH, Sadigh, B (2006) First-passage monte carlo algorithm: diffusion without all the hops. *Phys Rev Lett* 97:230602.
- [6] Gillespie, DT (1977) Exact stochastic simulation of coupled chemical reactions. *J Phys Chem* 81:2340.
- [7] Agmon, N and Szabo, A (1990) Theory of reversible diffusion-influenced reactions. *J Chem Phys* 92:5270 – 5284.